

AD-A161 390

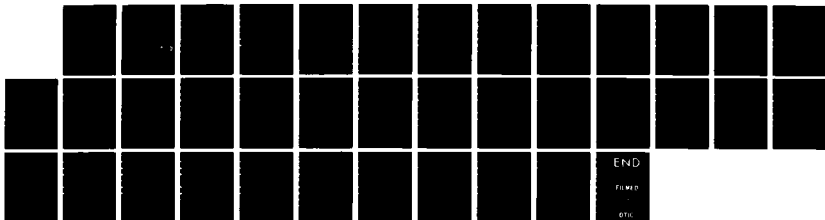
BEHAVIOR OF SINGLET OXYGEN IN THE OXYGEN-IODINE  
TRANSFER LASER(U) AEROSPACE CORP EL SEGUNDO CA  
AEROPHYSICS LAB R F HEIDNER 28 SEP 85 TR-0084(4610)-3  
SD-TR-85-65 F04701-83-C-0084

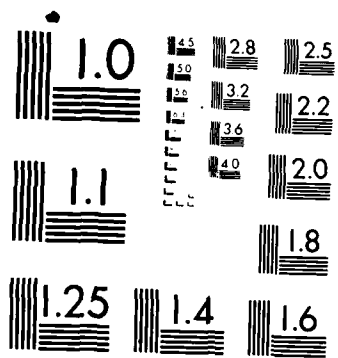
1/1

UNCLASSIFIED

F/G 7/5

NL





MICROCOPY RESOLUTION TEST CHART  
NATIONAL BUREAU OF STANDARDS 1963 A

12

AD-A161 390

# Behavior of Singlet Oxygen in the Oxygen-Iodine Transfer Laser

R. F. HEIDNER III  
Aerophysics Laboratory  
Laboratory Operations  
The Aerospace Corporation  
El Segundo, Calif. 90245

28 September 1985

APPROVED FOR PUBLIC RELEASE;  
DISTRIBUTION UNLIMITED

DTIC  
SELECTED  
NOV 20 1985  
S A D

Prepared for  
AIR FORCE WEAPONS LABORATORY  
Kirtland Air Force Base, N. Mex. 87117

DTIC FILE COPY

SPACE DIVISION  
AIR FORCE SYSTEMS COMMAND  
Los Angeles Air Force Station  
P.O. Box 92960, Worldway Postal Center  
Los Angeles, Calif. 90009-2960

11 18-85 004

This report was submitted by The Aerospace Corporation, El Segundo, CA 90245, under Contract No. F04701-83-C-0084 with the Space Division, P.O. Box 92960, Worldway Postal Center, Los Angeles, CA 90009-2960. It was reviewed and approved for The Aerospace Corporation by W. P. Thompson, Director, Aerophysics Laboratory. Lt. Colonel William E. McDermott, SD/YNS, was the Air Force project officer.

This report has been reviewed by the Public Affairs Office (PAS) and is releasable to the National Technical Information Service (NTIS). At NTIS, it will be available to the general public, including foreign nationals.

This technical report has been reviewed and is approved for publication. Publication of this report does not constitute Air Force approval of the report's findings or conclusions. It is published only for the exchange and stimulation of ideas.



WILLIAM E. MC DERMOTT, Lt Col, USAF  
Air Force Project Officer  
SD/YNS



JOSEPH HESS, GM-15  
Director, AFSTC West Coast Office  
AFSTC/WCO OL-AB

UNCLASSIFIED

SECURITY CLASSIFICATION OF THIS PAGE(When Data Entered)

19. KEY WORDS (Continued)

20. ABSTRACT (Continued)

into atoms. In the latter case, energy pooling between  $O_2(^1\Delta)$  and  $I^*$  is the dominant process unless a strong  $I^*$  quencher (e.g.,  $H_2O$ ) is present. In the former case, the  $O_2(^1\Delta)$ -driven chain reaction mechanism for  $I_2$  dissociation is the dominant feature of the kinetics. A detailed description of each of these regimes is critical in understanding the oxygen-iodine laser.

UNCLASSIFIED

SECURITY CLASSIFICATION OF THIS PAGE(When Data Entered)

UNCLASSIFIED

SECURITY CLASSIFICATION OF THIS PAGE (When Data Entered)

REPORT DOCUMENTATION PAGE		READ INSTRUCTIONS BEFORE COMPLETING FORM
1. REPORT NUMBER SD-TR-85-65	2. GOVT ACCESSION NO. AD-A161396	3. RECIPIENT'S CATALOG NUMBER
4. TITLE (and Subtitle) BEHAVIOR OF SINGLET OXYGEN IN THE OXYGEN-IODINE TRANSFER LASER		5. TYPE OF REPORT & PERIOD COVERED
		6. PERFORMING ORG. REPORT NUMBER TR-0084(4610)-3
7. AUTHOR(s)  Raymond F. Heidner III		8. CONTRACT OR GRANT NUMBER(s)  FO4701-83-C-0084
		10. PROGRAM ELEMENT, PROJECT, TASK AREA & WORK UNIT NUMBERS
9. PERFORMING ORGANIZATION NAME AND ADDRESS The Aerospace Corporation El Segundo, Calif. 90245		12. REPORT DATE 28 September 1985
11. CONTROLLING OFFICE NAME AND ADDRESS Air Force Weapons Laboratory Kirtland Air Force Base, N.M. 87117		13. NUMBER OF PAGES 31
		15. SECURITY CLASS. (of this report)  Unclassified
14. MONITORING AGENCY NAME & ADDRESS (if different from Controlling Office) Space Division Los Angeles Air Force Station Los Angeles, Calif. 90009-2960		15a. DECLASSIFICATION/DOWNGRADING SCHEDULE
16. DISTRIBUTION STATEMENT (of this Report)  Approved for public release; distribution unlimited.		
17. DISTRIBUTION STATEMENT (of the abstract entered in Block 20, if different from Report)		
18. SUPPLEMENTARY NOTES		
19. KEY WORDS (Continue on reverse side if necessary and identify by block number) Chemical Kinetics                      Flow Tube Kinetics Chemical Laser                          Iodine Atoms Electronically Excited Oxygen        Laser Photochemistry		
20. ABSTRACT (Continue on reverse side if necessary and identify by block number) The kinetic processes that affect the decay of $O_2(^1\Delta)$ in the oxygen-iodine transfer laser (COIL) are discussed. The kinetics of $O_2$ removal in the absence of iodine are now quite well established. A brief review of this topic is presented.  When $I_2$ is added to $O_2^*$ , a distinction can be made between the behavior of $O_2^*$ when $I_2$ and iodine atoms are present and when $I_2$ is fully dissociated		

## ACKNOWLEDGMENTS

I would like to thank my coworkers in the Aerophysics Laboratory:  
Dr. J. B. Koffend, Mr. G. I. Segal, Mr. C. E. Gardner, Mr. T. M. El-Sayed, and  
Dr. J. V. V. Kasper. Many of the conclusions represent technical discussions  
over several years with Dr. H. V. Lilienfeld of McDonnell Douglas Research  
Laboratory, Profs. P. L. Houston and J. R. Wiesenfeld of Cornell University,  
and Drs. D. J. Benard and A. T. Pritt, Jr., of Rockwell Science Center. I  
gratefully acknowledge both the support of and consultation with the members  
of the Advanced Laser Branch of the Air Force Weapons Laboratory.

## CONTENTS

ACKNOWLEDGMENTS.....	1
I. INTRODUCTION.....	9
II. EXPERIMENTAL.....	13
III. RESULTS AND ANALYSIS.....	17
A. Decay of $O_2(^1\Delta)$ in the Absence of $I_2$ and I.....	17
B. Decay of $O_2(^1\Delta)$ in I and $I^*$ ( $[I_2] = 0$ ).....	18
C. Decay of $O_2(^1\Delta)$ in I, $I^*$ , and $I_2$ .....	28
D. Extension to Photoinitiated $O_2^*$ - HI Mixtures.....	32
IV. CONCLUSION.....	35
REFERENCES.....	37

Location For	
NBS CR-6d	<input checked="" type="checkbox"/>
DTIC TAB	<input type="checkbox"/>
Unannounced	<input type="checkbox"/>
Justification	
By	
Date	
Availability Codes	
Available for	
Distribution	

A-1

## FIGURES

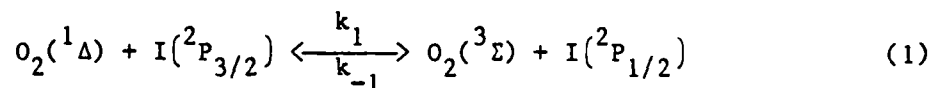
1.	Low-Lying Electronic Energy Levels and Observed Spectral Emissions for the $O_2$ and $I_2$ Molecules and the I Atom.....	10
2.	Schematic Diagram of the Computer-Controlled Kinetic Flow Tube Apparatus.....	14
3.	Schematic Diagram of the Excimer Photolysis Flow Tube Apparatus.....	15
4.	$I^*$ Decay Profiles as a Function of $[H_2O]$ .....	22
5a.	Decay of $O_2(^1\Delta)$ at High $I^*$ Density.....	25
5b.	Data of Fig. 5a Plotted as a Pure Second-Order Decay Process.....	26
6.	Plot of the First-Order (D) and Second-Order (C) Decay Coefficients as a Function of $[I]/[^3\Sigma]$ .....	27
7.	Removal of $O_2(^1\Delta)$ During $I_2$ Dissociation.....	31
8.	Normalized $I^*$ Decay Curves in $O_2^*$ vs. $[HI]_0$ .....	34

TABLES

1.	Rate Coefficient Data for $O_2(^1\Delta)$ Quenching in Pure $O_2$ (T = 295 K).....	19
2.	Rate Coefficient Data for $O_2(^1\Delta)$ Behavior in the Presence of $I^*$ and I.....	23
3.	Fractional Depletion of $O_2(^1\Delta)$ in the $I_2$ Dissociation Process: Mean Dissociation Efficiency, E, vs. $[^1\Delta]_0/[I_2]_0$ .....	33

## I. INTRODUCTION

The chemical oxygen-iodine laser (COIL)<sup>1-3</sup> is based on transferring energy from a majority energy storage species [ $O_2(^1\Delta)$ ] to a minority receptor species ( $I(^2P_{3/2})$ ):

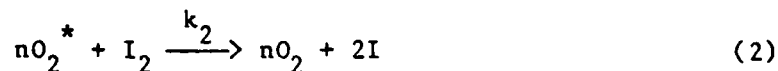


$$K_{EQ} = k_1/k_{-1} = 2.9 \text{ at } T = 295 \text{ K}$$

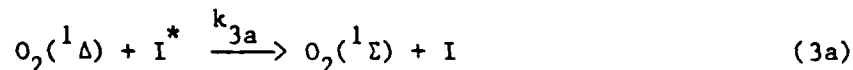
An energy level diagram for the low-lying electronic states of  $O_2$ ,  $I_2$ , and  $I$  is shown in Fig. 1. Examination of the above electronic state equilibrium and the threshold criterion for the atomic iodine laser ( $[I^*]/[I] > 0.5$ ) yields the conclusion that  $[O_2(^1\Delta)]/[O_2(^3\Sigma)] > 0.17$  in order to sustain cw laser oscillation. While the yield of  $O_2(^1\Delta)$  from the reaction of  $Cl_2$  and basic hydrogen peroxide is extremely high, deactivation of  $O_2(^1\Delta)$  to  $O_2(^3\Sigma)$  quickly degrades the extractable energy from such a device.

Direct quenching of  $O_2(^1\Delta)$  is extremely deleterious to laser performance; fortunately, most  $O_2(^1\Delta)$  quenching processes are extremely inefficient. Quenching of  $I^*$  is important because Process (1) connects the  $O_2(^1\Delta)$  energy storage reservoir with the  $I^*$  lasing medium.  $I^*$  quenching processes become significant loss mechanisms for  $O_2(^1\Delta)$  at high ratios of  $I^*/O_2(^1\Delta)$ .

In the review to follow, particular attention will be paid to the mechanism by which  $O_2^*$  dissociates molecular  $I_2$



and to the second-order energy pooling ( $k_{3a}$ ) and electronic quenching ( $k_{3b}$ ,  $k_{3c}$ , and  $k_{3d}$ ) processes.



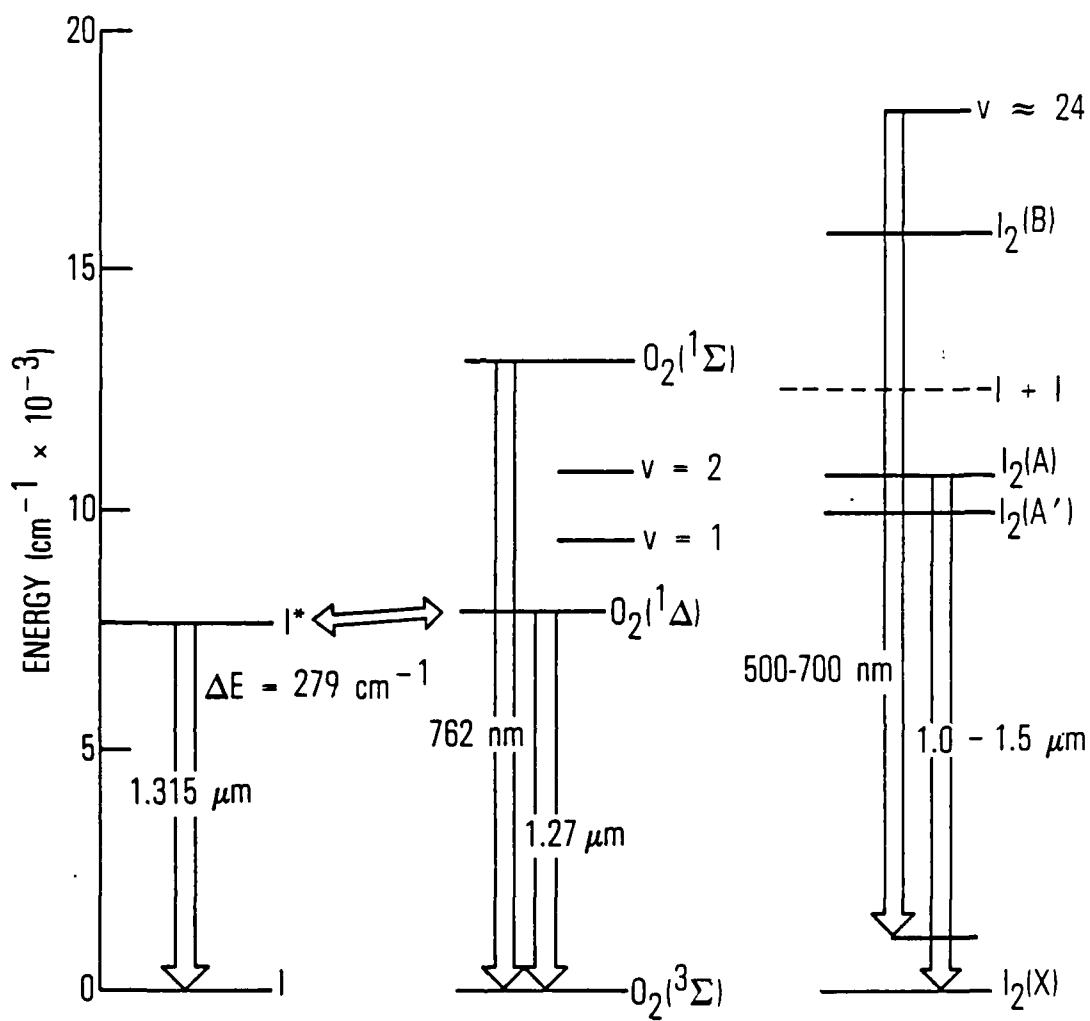


Fig. 1. Low-Lying Electronic Energy Levels and Observed Spectral Emissions for the  $O_2$  and  $I_2$  Molecules and the I Atom.



In the conventional COIL device, these processes are intrinsic loss processes for  $O_2(^1\Delta)$  that must be tolerated. Finally, we will briefly examine the advantages of replacing  $I_2$  by an alternate I-atom precursor that is premixable with  $O_2(^1\Delta)$ .

## II. EXPERIMENTAL

The work reported from the Aerophysics Laboratory of The Aerospace Corporation has been performed on two different experimental systems. The kinetic flow tube apparatus (Fig. 2) has been described in great detail in Ref. 4. The excimer laser photolysis apparatus (Fig. 3) has been described in Ref. 5. In both cases,  $O_2^*$  is created by a microwave discharge in pure  $O_2$  [ $O_2(^1\Delta)/O_2(^3\Sigma) < 0.1$ ], and the  $O(^3P)$  atoms are removed on a heated  $HgO$  surface just downstream of the discharge.

Although the apparatus in Fig. 3 is a flow system, the time histories of the important densities are monitored by time-resolved emission spectroscopy following the excimer laser photolysis pulse. In the apparatus of Fig. 2, steady-state emission intensities are monitored as a function of distance down the flow tube in order to extract kinetic information. In each case, the  $[O_2(^1\Delta)]$  is calibrated absolutely by isothermal calorimetry, and the  $[I^*]$  related to it by the ratio of the Einstein coefficients. Concentrations of  $O_2(^1\Sigma)$ ,  $I_2(A^3\Pi_{1u})$ , and  $I_2(B^3\Pi_{0+})$  were also followed during some experiments. Two experimental details are worth emphasizing. First, the treatment of the walls in the flow tube apparatus were coated with a low melting halogenated wax (Halocarbon, Inc.) that was very inefficient at recombining I atoms. Secondly, the use of an extremely sensitive intrinsic Ge detector (ADC 403 HS) permitted the detection of  $O_2(^1\Delta)$  and  $I^*$  in the flow tube with excellent S/N and  $I^*$  with good time response in the excimer photolysis apparatus.

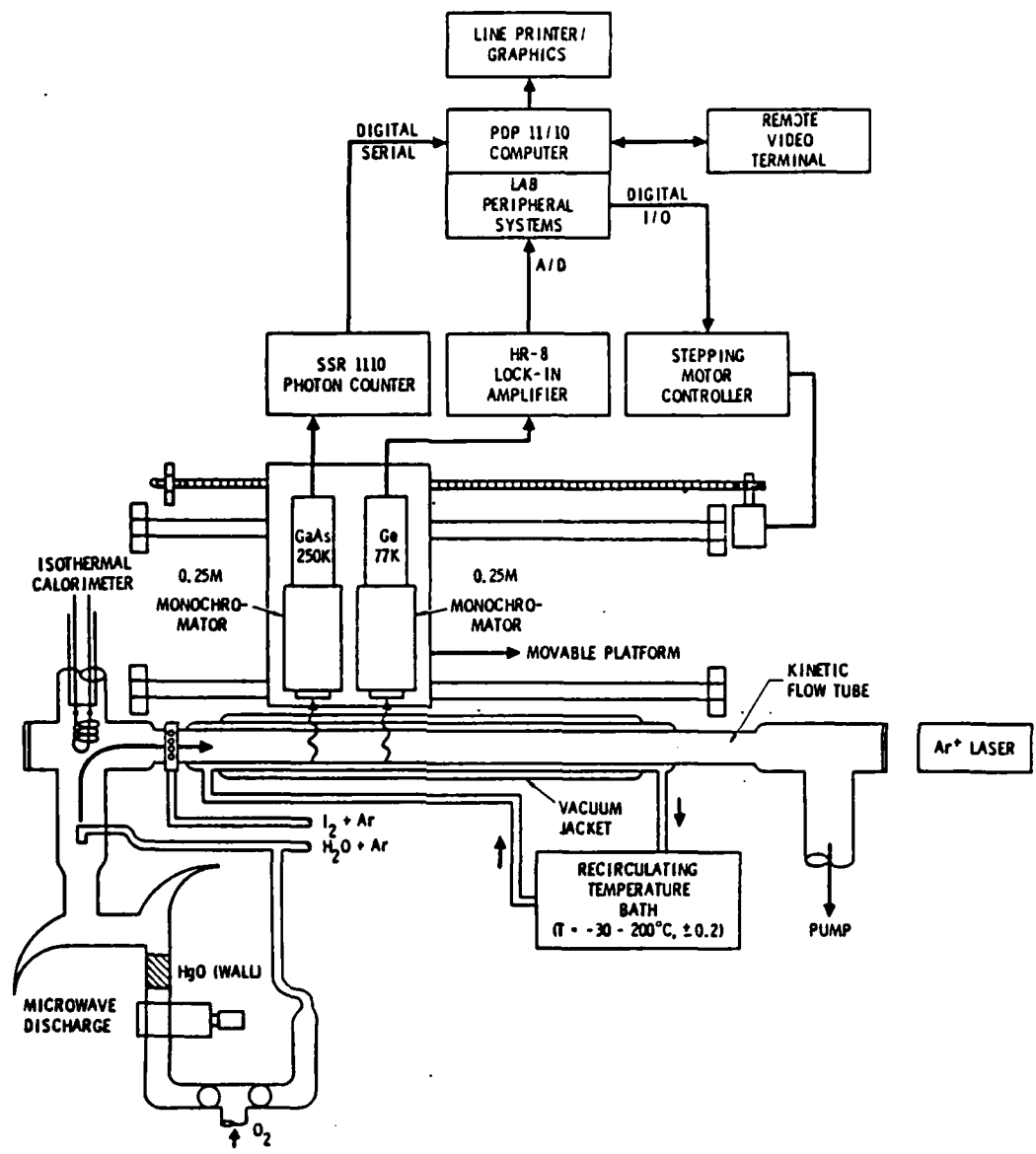


Fig. 2. Schematic Diagram of the Computer-Controlled Kinetic Flow Tube Apparatus.

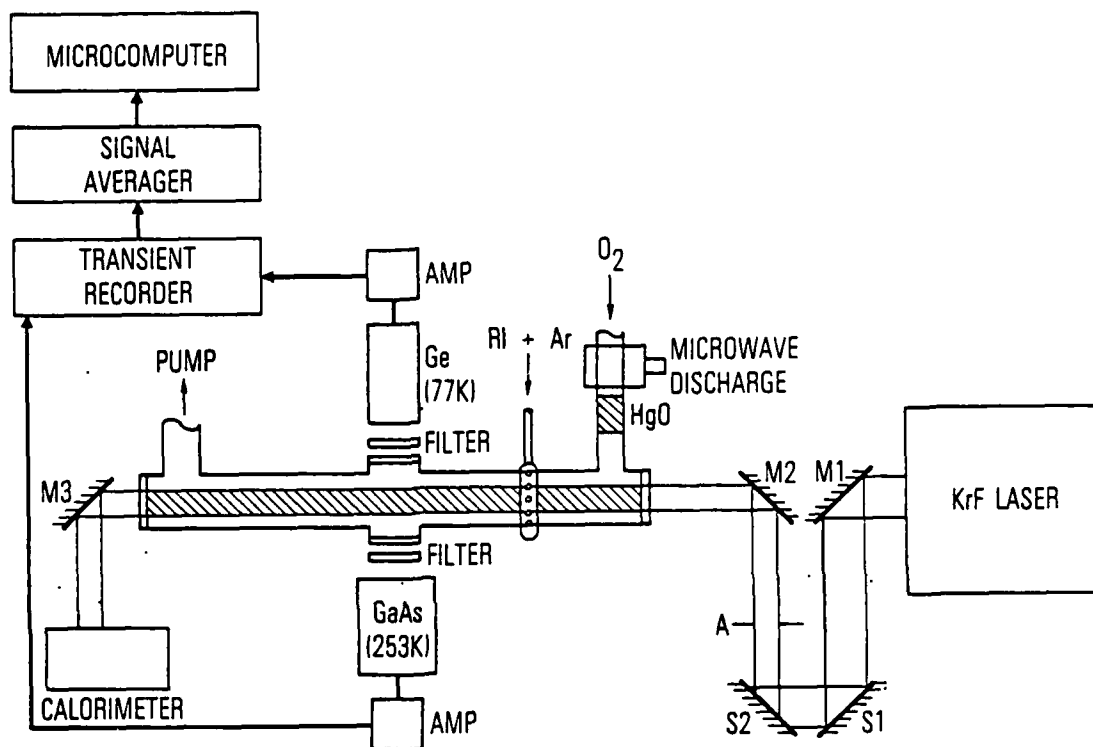
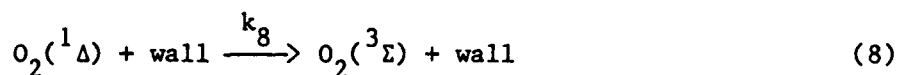
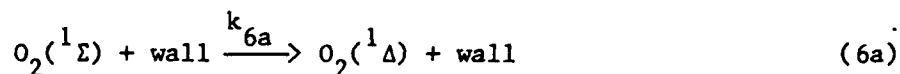
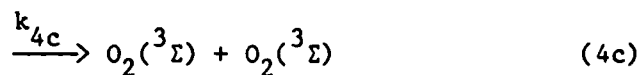
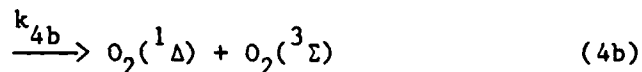
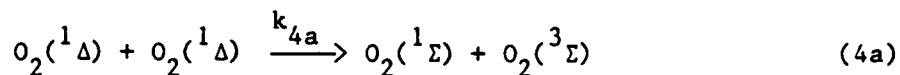


Fig. 3. Schematic Diagram of the Excimer Photolysis Flow Tube Apparatus.

### III. RESULTS AND ANALYSIS

#### A. DECAY OF $O_2(^1\Delta)$ IN THE ABSENCE OF $I_2$ AND $I$

The decay of  $O_2(^1\Delta)$  can be accurately described by a combined first- and second-order decay equation based on the following processes:



The solution can be written as follows:

$$[O_2(^1\Delta)]^{-1} = \{[O_2(^1\Delta)]_0^{-1} + \frac{A}{B}\} \exp(Bt) - \left(\frac{A}{B}\right) \quad (9)$$

$$\text{where } A = 2k_{4a} - \left\{ \frac{k_{4a}(k_{5a} + k_{6a})}{(k_5 + k_6)} \right\} + k_{4b} + 2k_{4c}$$

$$\text{and } B = k_8 + k_7^M[M].$$

Making the assumption that  $O_2(^1\Sigma)$  is quenched predominantly to  $O_2(^1\Delta)$  and that the two dominant quenchers from a COIL chemical generator are  $O_2(^3\Sigma)$  and  $H_2O$ , we can write

$$A = k_{4a} + k_{4b} + 2k_{4c}$$

$$B = k_8 + k_7^{O_2} [O_2(^3\Sigma)] + k_7^{H_2O} [H_2O]$$

The necessary rate coefficient information for evaluating  $O_2(^1\Delta)$  decays under these conditions is shown in Table 1. Because the rate coefficient  $k_4$  is so small, it is extremely difficult to detect the second-order decay component in a pure  $O_2$  or an  $O_2 + H_2O$  system.

B. DECAY OF  $O_2(^1\Delta)$  IN I and  $I^*$  ( $[I_2] = 0$ )

1. DECAY OF CURVES FOR  $[O_2(^1\Delta)] \gg [O_2(^3\Sigma)]$

Under conditions that are approachable with a chemical generator for singlet oxygen, the relationship between  $O_2(^1\Delta)$  and  $I^*$  can be written as follows<sup>4</sup>:

$$[I^*] = \frac{(2X) [I_2]_0}{(1 + X)} \quad (10)$$

where  $X = K_{EQ} [^1\Delta] / [^3\Sigma] = [I^*] / [I]$ . In this case, since  $X \gg 1$ ,  $[I^*] = 2[I_2]_0$ , i.e., all the I atoms are in the excited state. Thus,  $[I^*]$  can be treated as one of the constant quenchers in Eq. (7).

2. DECAY CURVES FOR  $[O_2(^1\Delta)] = (0.1 - 1.0) [O_2(^3\Sigma)]$

In this important region for the chemical laser, analytic modeling is complicated, and numerical methods are to be preferred.

3. DECAY CURVES FOR  $[O_2(^1\Delta)] < 0.1 [O_2(^3\Sigma)]$

In this regime where flow tube experiments employing microwave discharge production of  $O_2^*$  operate, Eq. (10) reduces to

$$[I^*] = \frac{2K_{EQ} [^1\Delta] [I_2]_0}{[O_2]_{tot} + 1.9[^1\Delta]} \sim C [^1\Delta] \quad (11)$$

Table 1. Rate Coefficient Data for  $O_2(^1\Delta)$  Quenching  
in Pure  $O_2$  (T = 295 K)

Process	M	Rate Coefficient ( $cm^3/molecule\text{-}sec$ )	References
$k_{4a}$		$(2.0 \pm 0.5) \times 10^{-17}$	6
		$(2.0 \pm 0.6) \times 10^{-17}$	8
$k_4$		$< 5 \times 10^{-17}$	7
$k_5$	$O_2$	$(4.0 \pm 0.4) \times 10^{-17}$	9
		$(3.9 \pm 0.2) \times 10^{-17}$	10
	$H_2O$	$(5 \pm 1) \times 10^{-12}$	11
		$4.7 \times 10^{-12}$	12
		$(6.7 \pm 0.5) \times 10^{-12}$	13
$k_6$	$\gamma^a =$	$1 \times 10^{-2}$ (pyrex)	6
		$2 \times 10^{-2}$ (pyrex)	8
		$1 \times 10^{-3}$ (Halocarbon)	8
$k_7$	$O_2$	$(1.6 \pm 0.05) \times 10^{-18}$	14
		$(1.5 \pm 0.05) \times 10^{-18}$	15
	$H_2O$	$(4 \pm 1) \times 10^{-18}$	11
$k_8$	$\gamma^a =$	$2 \times 10^{-5}$ (pyrex)	6
		$1.2 \times 10^{-5}$ (pyrex)	14
		$3 \times 10^{-5}$ (Halocarbon)	8

<sup>a</sup> $\gamma$  represents the wall recombination probability;  $\gamma = (2Rk)/c$  in a cylindrical flow tube;  $c$  is the oxygen mean velocity;  $R$  is the tube radius; and  $k$  is the measured removal rate ( $sec^{-1}$ ).

where  $[I^*]$  is directly proportional to  $O_2(^1\Delta)$ . For this last case, we can write an  $O_2(^1\Delta)$  decay equation analogous to Eq. (9) based on an analysis originally put forth by Derwent and Thrush<sup>16</sup>:

$$[O_2(^1\Delta)]^{-1} = \{[O_2(^1\Delta)]_0^{-1} + \frac{C}{D}\} \exp(Dt) - \frac{C}{D} \quad (12)$$

where

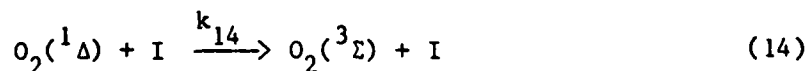
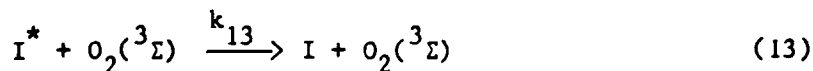
$$\begin{aligned} C &= A + \frac{k_1}{(k_{-1} + k_{13})} (k_{3a} + 2k_{3b} + k_{3c} + k_{3d}) \frac{[I]}{[{}^3\Sigma]} \\ &= A + K_{EQ}(k_{3a} + 2k_{3b} + k_{3c} + k_{3d}) \frac{[I]}{[{}^3\Sigma]} \end{aligned}$$

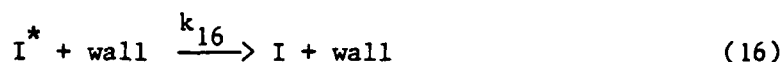
and

$$\begin{aligned} D &= B + \left\{ k_{14} + \frac{k_{13}k_1 + k_1(k_{15}^M [M] + k_{16} + k_{17})/[{}^3\Sigma]}{(k_{-1} + k_{13})} \right\} [I] \\ D &= B + \left\{ k_{14} + K_{EQ}(k_{13} + (k_{15}^M [M] + k_{16} + k_{17})/[{}^3\Sigma]) \right\} [I] \\ &= B + \left\{ k_{eff} + K_{EQ}(k_{15}^M [M] + k_{16} + k_{17})/[{}^3\Sigma] \right\} [I] \end{aligned}$$

$$k_{eff} = k_{14} + K_{EQ}k_{13}$$

The terms A and B were defined in Eq. (9). The term  $k_{eff}$  was introduced by Derwent and Thrush<sup>16</sup> and has been used subsequently by other authors<sup>8</sup> in order to analyze their data. The additional processes introduced above are defined as follows:





We will show that  $k_{-1} \gg k_{13}$  allowing  $K_{EQ}$  to replace the term  $k_1/(k_{-1} + k_{13})$  in the definitions of C and D above. Figure 4, taken from Ref. 17, shows that using  $H_2O$  as an  $I^*$  quencher that one observes qualitatively a regime where first- and second-order components are both significant  $[(H_2O) = 0]$ . Upon the addition of  $H_2O$ , one begins to see single exponential decays. As noted in Ref. 17, the derived value of  $k_{15}^{H_2O} = 1.7 \times 10^{-12} \text{ cm}^3/\text{molecule-sec}$  is in good agreement with literature values (Table 2).

As is the typical case for combined first- and second-order decays, an unambiguous deconvolution is very difficult without exceedingly precise data. This system is no exception to that rule. Derwent and Thrush<sup>16</sup> concluded that the second-order component of the  $O_2(^1\Delta)$  decay in the presence of  $I^*$  was not observable, however, our studies are not consistent with that conclusion.

In Fig. 5a, we see an  $O_2(^1\Delta)$  decay curve versus time taken in our kinetic flow tube. A two parameter nonlinear least squares fit to these data is superimposed. In Fig. 5b, the data are plotted as though they represent a pure second-order decay. The first-order wall decay (measured without I atoms) is exceedingly small and, clearly, the incremental first-order decay component in the presence of I and  $I^*$  is small as well. It should be noted that the relative  $[O_2(^1\Delta)]$  must be determined by obtaining a difference spectrum since  $I_2(A^3\Pi_{1u} \rightarrow X^1\Sigma)$  emission overlaps the  $O_2(a^1\Delta \rightarrow X^3\Sigma)$  emission band. Analysis of the C and D coefficients in Eq. (12) as a function of  $[I]/[^3\Sigma]$  gives the plot in Fig. 6. From it, we estimate that  $k_{3a} + 2k_{3b} + k_{3c} + k_{3d} = 2.1 \times 10^{-13} \text{ cm}^3/\text{molecule-sec}$ . The rate coefficient  $k_{3a}$  has been measured to be  $\sim 1 \times 10^{-13} \text{ cm}^3/\text{molecule-sec}$  (Table 2). Upon addition of  $I_2$ , we find that the increase in the first-order decay coefficient, i.e. (D-B), is not statistically significant. Using the value  $(D-B) < 0.13 \text{ sec}^{-1}$  gives the following inequality:

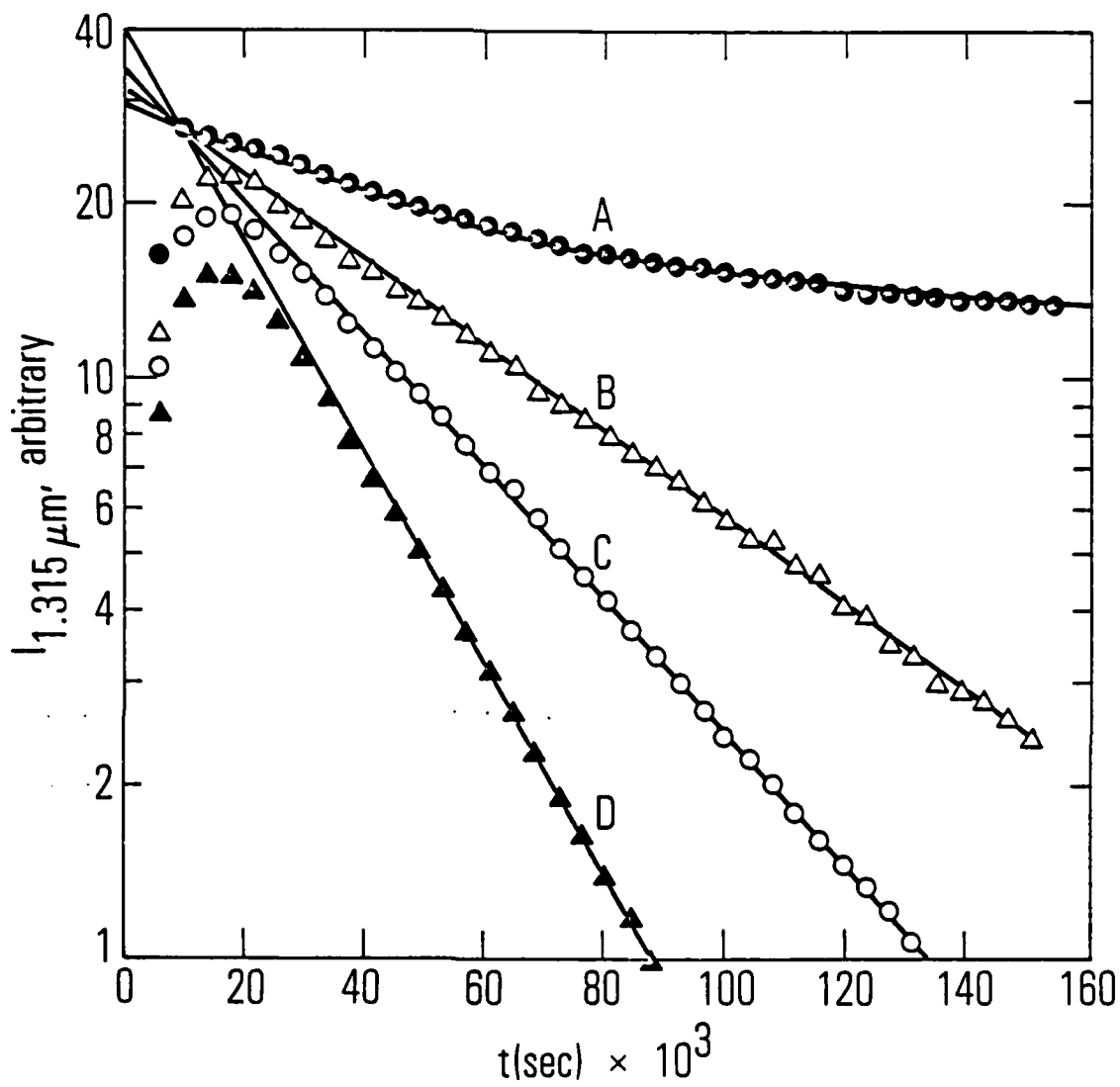


Fig. 4.  $I^*$  Decay Profiles as a Function of  $[H_2O]$ . (These profiles mimic  $[O_2(^1\Delta)]$  decays.) Experimental conditions:  $P = 3.15$  Torr,  $[^1\Delta]_0 = 6.5 \times 10^{15}$ ,  $[^3\Sigma]_0 = 7.4 \times 10^{16}$ ,  $[I_2]_0 = 7.1 \times 10^{13}$  molecules/cm<sup>3</sup>. Curves A - D:  $[H_2O] = 0, 1.0 \times 10^{15}, 2.1 \times 10^{15},$  and  $4.1 \times 10^{15}/\text{cm}^3$  ( $[Ar] = \text{balance}$ ).

Table 2. Rate Coefficient Data for  $O_2(^1\Delta)$  Behavior in the Presence of  $I^*$  and I

Process	M	Rate Coefficient ( $cm^3/molecule\text{-}sec$ )	References
$k_{-1}$		$(2.7 \pm 0.3) \times 10^{-11}$	18
$(k_1)$		$(7.8 \pm 0.8) \times 10^{-11}$	a
$k_{3a}$		$2.7 \times 10^{-14}$ ( $1.3 \times 10^3$ )	6,16 <sup>b</sup>
		$8 \times 10^{-14}$ ( $4 \times 10^3$ )	8 <sup>b</sup>
		$1.1 \times 10^{-13}$ ( $5.5 \times 10^3$ )	19 <sup>b,c</sup>
		$8.4 \times 10^{-14}$ ( $4.2 \times 10^3$ )	19 <sup>b,c</sup>
$k_3$		$2.1 \times 10^{-13}$	This Work
$k_{eff}^d$		$1.3 \times 10^{-13}$	6
		$3 \times 10^{-14}$	8
		$< 1 \times 10^{-15}$	This Work
$k_{13}$		$4.6 \times 10^{-14}$	6
		$1 \times 10^{-14}$	8
		$< 3.5 \times 10^{-16}$	This Work
		$(0.9 \pm 4) \times 10^{-12}$	18
$k_{14}$		$1.3 \times 10^{-13}$	6
		$3 \times 10^{-14}$	8
		$< 1 \times 10^{-15}$	This Work
$k_{15}$	$H_2O$	$(2.5 \pm 0.5) \times 10^{-12}$	20
	.	$(2.1 \pm 0.3) \times 10^{-12}$	21
	.	$1.7 \times 10^{-12}$	17
	$I(^2P_{3/2})$	$< 1.7 \times 10^{-13}$	This Work
		$< 1.6 \times 10^{-14}$	22

Table 2. Rate Coefficient Data for  $O_2(^1\Delta)$  Behavior in the Presence of  $I^*$  and I (Continued)

Process	M	Rate Coefficient ( $cm^3/molecule\text{-}sec$ )	References
$k_{16}$		$< 30 \text{ sec}^{-1e}$	This Work
$k_{17}$		$< 30 \text{ sec}^{-1}$ $7.8 \text{ sec}^{-1}$	This Work 23

<sup>a</sup>The forward rate coefficient,  $k_1$ , is determined by the reverse rate coefficient and the equilibrium constant,  $K_{EQ}$ .

<sup>b</sup>The values in parentheses are the measured ratios of  $k_{3a}/k_{3b}$ .

<sup>c</sup>The quoted values were obtained in Ref. 19 by alternate methods for calculating the I atoms in the system.

<sup>d</sup>The term  $k_{eff}$  is determined in the text as a combination of rate coefficients.

<sup>e</sup>The diffusion rate to the wall in this system is calculated to be  $40 \text{ s}^{-1}$  from the diffusion equation for a long cylinder and using a diffusion coefficient of  $0.1 \text{ cm}^2/\text{s}$ .

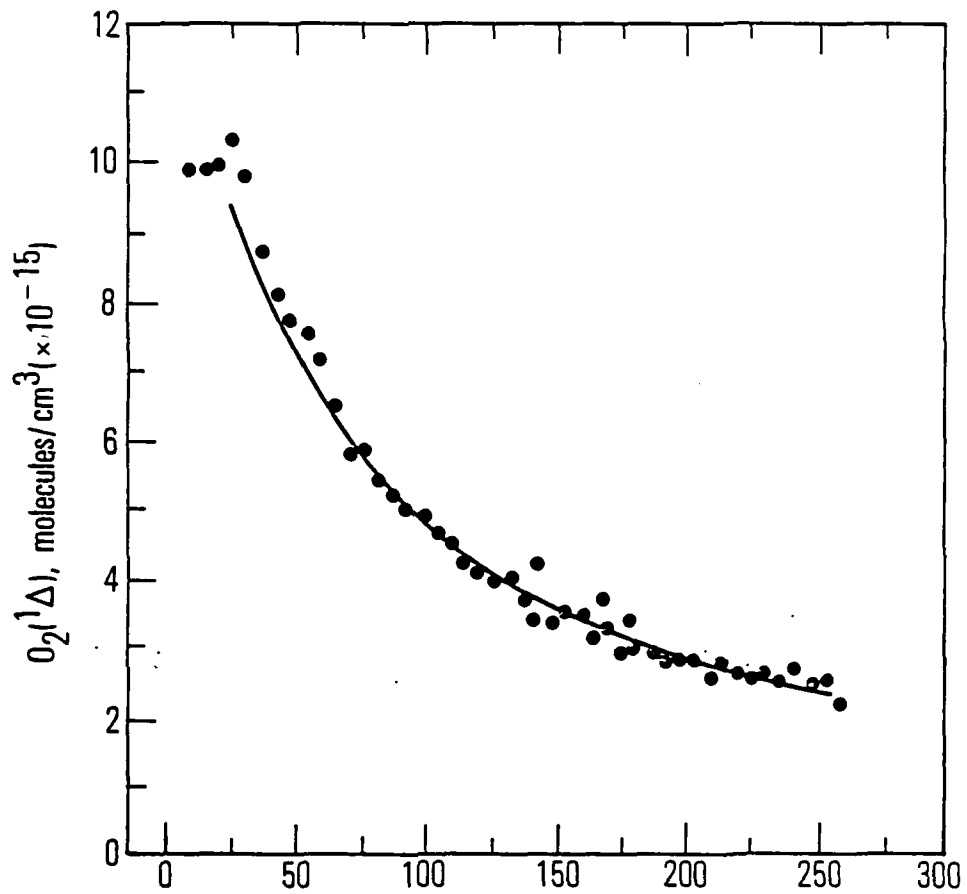


Fig. 5a. Decay of  $O_2(^1\Delta)$  at High  $I^*$  Density.  $[^1\Delta]_0 = 1.0 \times 10^{16}$  and  $[I_2]_0 = 1.98 \times 10^{13}/\text{cm}^3$ . Solid line is a fit to Eq. (12).

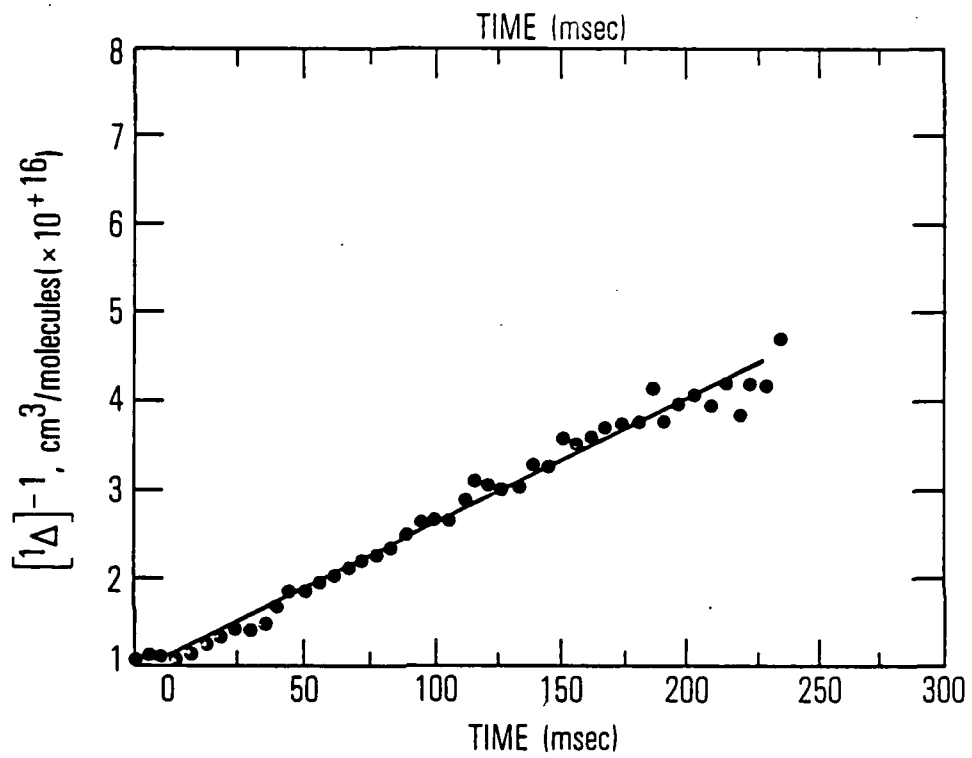


Fig. 5b. Data of Fig. 5a Plotted as a Pure Second-Order Decay Process.

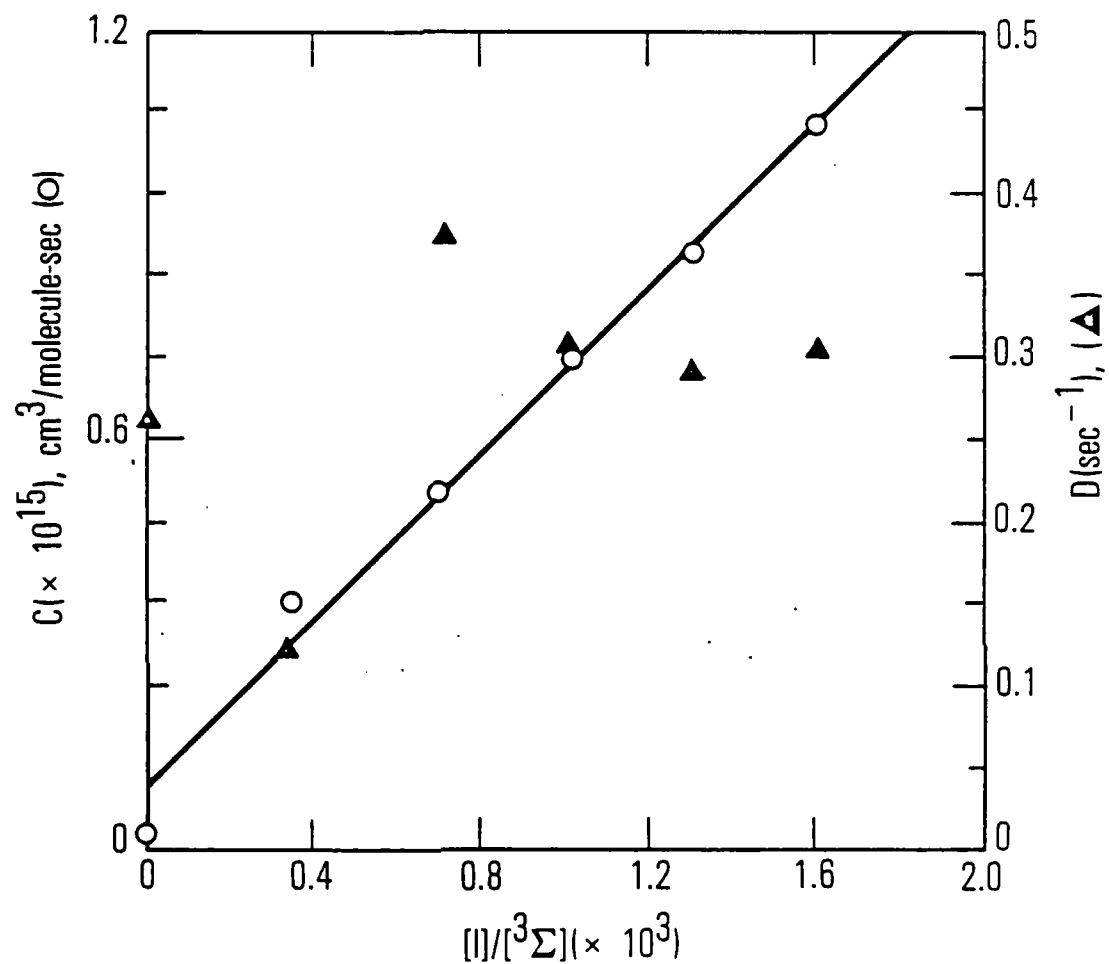


Fig. 6. Plot of the First-Order (D) and Second-Order (C) Decay Coefficients as a Function of  $[I]/[{}^3\Sigma]$  [see Eq. (12)].

$$k_{14} + K_{EQ} \{k_{13} + (k_{15} M [M] + k_{16} + k_{17}) / [{}^3\Sigma]\} < 1 \times 10^{-15} \text{ cm}^3/\text{sec}$$

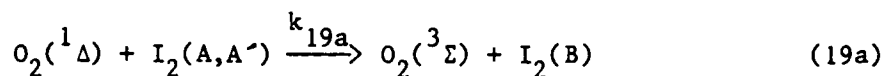
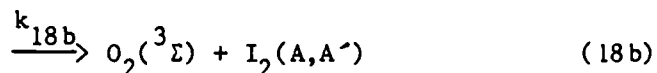
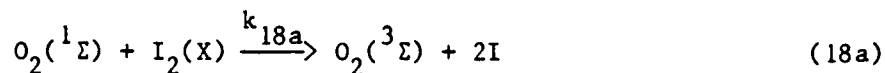
Using this inequality, we can derive the upper bounds for a number of first-order quenching processes that might be occurring in the COIL system. These rate coefficients are  $k_{14} < 1 \times 10^{-15}$ ,  $k_{13} < 3.3 \times 10^{-16}$  ( $\ll k_{-1}$ ), and  $k_{15}^I < 1.7 \times 10^{-13} \text{ cm}^3/\text{molecule-sec}$ . The rates  $k_{16} < 30 \text{ sec}^{-1}$  and  $k_{17} < 30 \text{ sec}^{-1}$  are determined as well. These upper bounds are considerably lower than those proposed by Derwent and Thrush<sup>16</sup> and are somewhat lower than those reported by Fisk and Hays.<sup>8</sup> The limit imposed upon  $k_{17}$  is a factor of four larger than the accepted spontaneous emission rate from  $I^*$  ( $A_{EIN} = 7.8 \text{ sec}^{-1}$ ).<sup>23</sup>

These results are offered as an example of the difficulty in deconvolving first- and second-order decays in a regime where their magnitudes are comparable. Although our results seem quite different from those of Fisk and Hays,<sup>8</sup> it should be realized that they represent a difference in rate increase of  $0.13 \text{ sec}^{-1}$  in one experiment and perhaps  $2 \text{ sec}^{-1}$  in the other. Neither experiment should be considered to be definitive in determining these small changes in such a complex system. Clearly, the second-order component of the decay plays a significant role based on independent evidence regarding the formation of  $O_2({}^1\Sigma)$ . On the basis of our own work, we believe that most of the I-atom catalyzed first-order decay processes for  $O_2({}^1\Delta)$  can be ignored. The exceptions are the quenching processes for  $I^*$ . The results of this study are compared to previous work in Table 2.

### C. DECAY OF $O_2({}^1\Delta)$ IN I, $I^*$ , and $I_2$

The stored energy in  $O_2^*$  is known to be capable of dissociating  $I_2$ . The efficiency of this dissociation process is thus a primary consideration for the design of a COIL device. Examination of the energy level diagram in Fig. 1 shows that two quanta of  $O_2({}^1\Delta)$  energy are required in order to break the  $I_2$  bond (35.1 kcal/mol).

One of the original suggestions made by Ogryzlo and coworkers<sup>24</sup> and endorsed by the extensive work of Derwent and Thrush<sup>25,26</sup> was that  $I_2$  was both excited and dissociated by  $O_2({}^1\Sigma)$ :

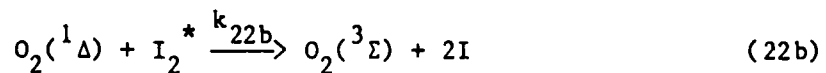
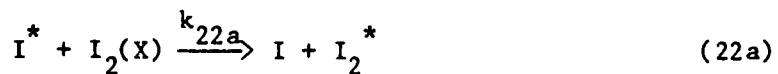
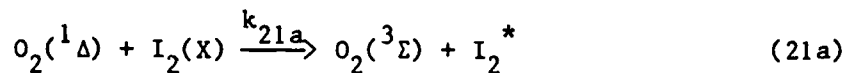


The  $\text{O}_2(^1\Sigma)$  is formed by Processes (3a) and (4). Although the details of the kinetic model that describes this mechanism are complex, the efficiency of the process in terms of  $\text{O}_2(^1\Delta)$  storage molecules consumed can be written down by inspection relative to an efficiency of 1.0 for the consumption of 2  $\text{O}_2(^1\Delta)$  molecules per  $\text{I}_2$  dissociated:

$$E = \frac{k_{18a}[\text{I}_2]}{(k_{18}[\text{I}_2] + k_5^M[\text{M}] + k_6)} \quad (20)$$

If  $\text{I}_2$  is the chief loss mechanism for  $\text{O}_2(^1\Sigma)$ , then the dissociation efficiency is given by  $E = k_{18a}/k_{18}$ , which has been measured to be  $< 0.2$ .<sup>27</sup> If there are other loss mechanisms for  $\text{O}_2(^1\Sigma)$ , the efficiency is lower still.

Although this mechanism may be operative in the COIL system, recent experiments<sup>17,27</sup> have shown that  $k_{18a}$  is too slow to account for the phenomenological dissociation rates of  $\text{I}_2$  in  $\text{O}_2^*$ . A sequential excitation model<sup>4</sup> for  $\text{I}_2$  dissociation can be proposed that is kinetically identical:



Either or both of the above sequences are kinetically acceptable, however, we prefer sequence (22) as it invokes collisions of the intermediate  $I_2^*$  with a majority flow species [ $O_2(^1\Delta)$ ] rather than a minority one ( $I^*$ ). Either high vibrational levels of  $I_2(X)$  or the electronically metastable  $I_2(A, A')$  states have been examined as candidates for the intermediate state in Processes (21) and (22). At present, there is qualitative support for all of the suggested intermediate states. Further quantitative work must be done. Assuming that Process (22) is responsible for the bulk of the  $I_2$  dissociation, the efficiency of  $O_2(^1\Delta)$  utilization is given by

$$E_{SQ} = \left\{ \frac{k_{22b}[^1\Delta]}{R_{I_2^*}} \right\} \left\{ \frac{k_{22a}[I_2]}{R_{I^*}} \right\} \quad (23)$$

where  $R_{I_2^*}$  is the total rate of intermediate removal ( $\text{sec}^{-1}$ ) and  $R_{I^*}$  is the total rate of  $I^*$  removal. Thus, the overall dissociation efficiency is the product of the  $I^*$  utilization efficiency in (22a) and the efficiency by which the  $I_2^*$  intermediate is used in (22b). It is interesting to note that COIL devices work well at  $[O_2(^1\Delta)]/[I_2]$  ratios of approximately 100 and that  $k_{22a}/k_3$  is approximately 300. We believe that  $k_{22b}[^1\Delta]/R_{I_2^*}$  must be close to unity,<sup>4</sup> although that may be an untenable assumption for a vibrationally excited  $I_2(X)$  intermediate.

Removal of  $O_2(^1\Delta)$  during the  $I_2$  dissociation process is quite difficult to quantify experimentally. A seemingly trivial problem in flow tube methodology has rather serious consequences. It is difficult to mix small amounts of  $I_2$  (MW 254) into a stream of  $O_2$  (MW 32) in an efficient manner. A carrier gas (typically Ar) is saturated with  $I_2$  (0.1 to 10%  $I_2$  in Ar) and injected into the  $O_2$  flow. We want to attain fast mixing and fast  $I_2$  dissociation in order to decouple this  $O_2(^1\Delta)$  loss from that caused by  $I$  and  $I^*$  (Section IIIB). In order to get fast mixing (i.e., on the timescale of the  $I_2$  dissociation), one has to inject an Ar +  $I_2$  mixture that represents roughly 5% of the  $O_2$  molar flow rate. As shown schematically in Fig. 7, this Ar then

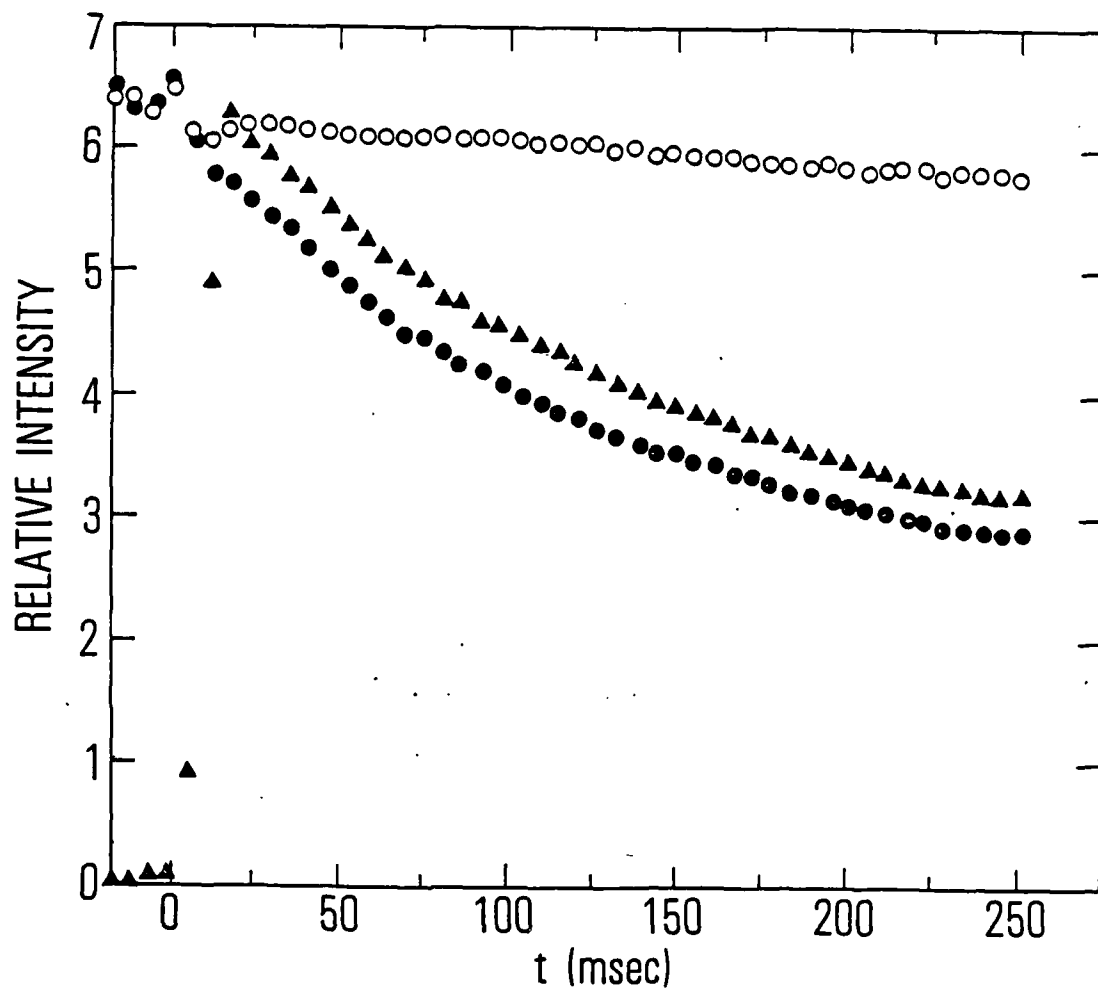


Fig. 7. Removal of  $O_2(^1\Delta)$  During  $I_2$  Dissociation. (O): dilution of  $O_2(^1\Delta)$  by injected Ar. (●) removal of  $O_2(^1\Delta)$  by injected Ar +  $I_2$ . (Δ): production of  $I^*$  during  $I_2$  dissociation. Conditions:  $[O_2(^1\Delta)]:[O_2(^3\Sigma)] = 5.2 \times 10^{15}: 7.7 \times 10^{16}$  molecules/cm<sup>3</sup>,  $[I_2]_0 = 5.7 \times 10^{13}$  molecules/cm<sup>3</sup> (●, Δ).

dilutes the  $O_2^*$  by 5% at the mixing point. In our system, it is impossible to measure an  $O_1(^1\Delta)$  decrease because of  $I_2$  dissociation of  $< 2\%$  in the presence of that dilution process. Table 3 is a matrix of percentage  $[O_2(^1\Delta)]$  decrease as a function of initial  $[^1\Delta]/[I_2]$  ratio and mean dissociation efficiency. The entries resulting in greater than 20% loss of  $O_2(^1\Delta)$  are omitted. The weak area of this method involves measuring efficiencies for large  $[^1\Delta]/[I_2]$  ratios. For ratios of  $10^4$ , we are tempted to assign a 2%  $O_2(^1\Delta)$  decrease to an efficiency of 0.01, however, that efficiency is properly expressed as  $[0.01 + 1.0 (-0.005)]$ .

Our own data are convincing for  $[^1\Delta]_0/[I_2]_0$  ratios of 100. It is shown that the dissociation efficiency is extremely high. We estimate that it is  $(0.75 \pm 0.25)$  or that  $(3 \pm 1)$   $O_2(^1\Delta)$  molecules are required to dissociate an  $I_2$ . Our results depend critically on the fact that the Halocarbon wax surface of the flow tube inhibits I atom recombination (and perhaps even  $I^*$  relaxation). Thus,  $I_2$  is not reformed on the walls by I atom recombination and redissociated by additional  $O_2(^1\Delta)$ . Results on  $O_2(^1\Delta)$  loss in the  $I_2$  dissociation regime clearly depend on wall and diffusional parameters of a particular experimental apparatus.

#### D. EXTENSION TO PHOTOINITIATED $O_2^*$ - HI MIXTURES

The decay of  $O_2(^1\Delta)$  in time-resolved kinetics experiments can be monitored by photodissociation of an I-atom precursor in the apparatus shown in Fig. 3. Although  $O_2(^1\Delta)$  is difficult to monitor directly in such experiments, one can monitor  $[I^*]$ , which is proportional to it under the proper conditions [Eq. (11)]. The precursor chosen (HI) has an extremely small quenching coefficient for  $O_2(^1\Delta)$ . The results of these experiments are detailed in Ref. 5. In the present context, the effect is shown by increasing the density of the precursor (Fig. 8) in order to increase the initial I atom concentration produced by the laser. At low precursor densities, it has been shown that the coupled  $I^* - O_2(^1\Delta)$  removal is dominated by a combination of axial diffusion, radial diffusion, and cell pumpout. As the initial  $[I] + [I^*]$  density increases, the removal does accelerate. Also, the acceleration is entirely consistent with Process (3). Thus, independent confirmation is available that the first-order I-atom-related loss processes for  $O_2(^1\Delta)$  are extremely small.

Table 3. Fractional Depletion of  $O_2(^1\Delta)$  in the  $I_2$  Dissociation Process: Mean Dissociation Efficiency, E, vs.  $[^1\Delta]_0/[I_2]_0$

Mean Dissociation Efficiency (E)	Fractional Depletion for the Following Values of $[O_2(^1\Delta)]_0/[I_2]_0$			
	10	$10^2$	$10^3$	$10^4$
1	0.2	0.02	$2 \times 10^{-3}$	$2 \times 10^{-4}$
0.1	-	0.2	0.02	$2 \times 10^{-3}$
0.01	-	-	0.2	0.02
0.001	-	-	-	0.2

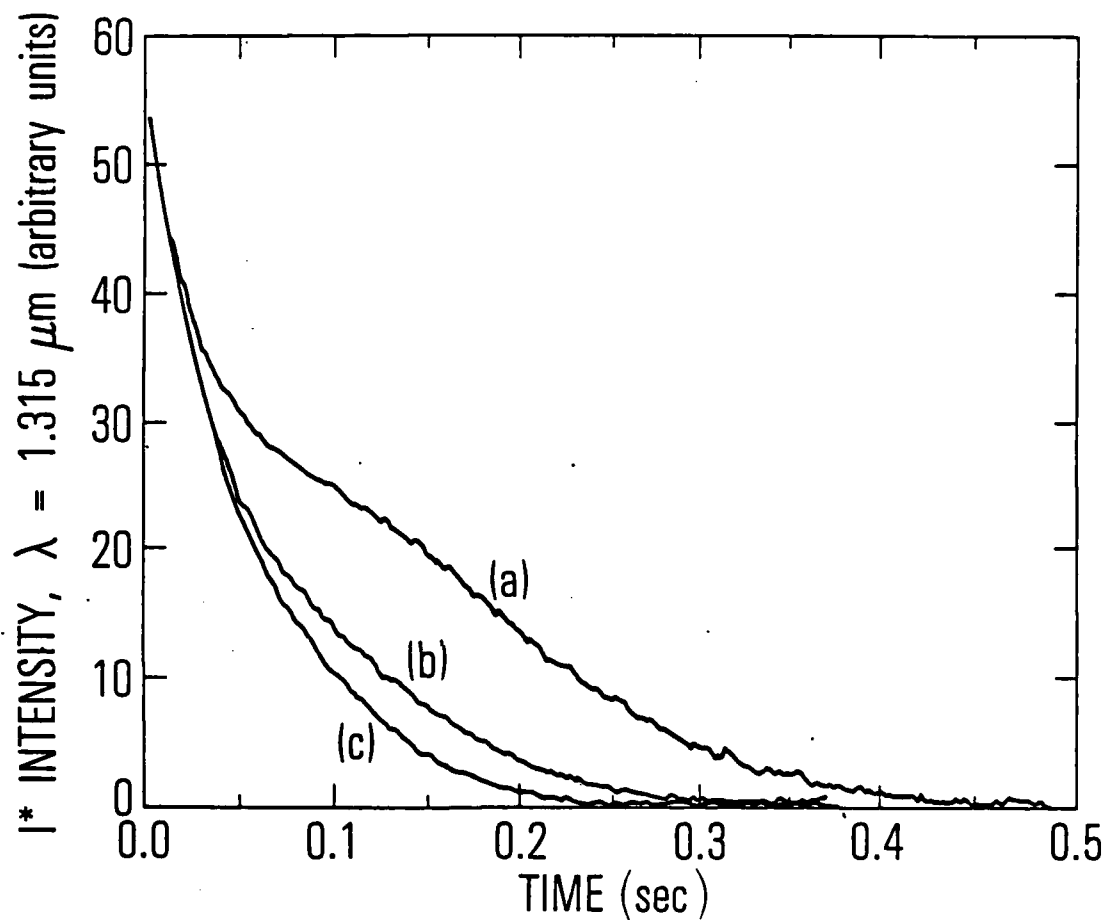


Fig. 8. Normalized  $I^*$  Decay Curves in  $O_2^*$  vs.  $[HI]_0$ .  $[^3\Sigma] = 9.0 \times 10^{16}$ , and  $[^1\Delta] = 7.9 \times 10^{15}/\text{cm}^3$ . Percentage photolysis of HI = 2.2%. Curves A-C:  $[HI]_0 = 6.4 \times 10^{14}$ ,  $2.5 \times 10^{15}$ , and  $4.4 \times 10^{15}/\text{cm}^3$ .

#### IV. CONCLUSION

The kinetic processes that remove  $O_2(^1\Delta)$  in a COIL system have been reviewed in this report. In the absence of  $I_2$ ,  $I^*$ , and  $I$ , the  $O_2(^1\Delta)$  decays very slowly by energy pooling [second order Process (4)], gas phase quenching by  $H_2O$  and  $O_2(^3\Sigma)$ , and by wall quenching.

The removal of  $O_2(^1\Delta)$  in the presence of  $I^*$  and  $I$  is described by introducing the energy pooling  $O_1(^1\Delta)$  with  $I^*$  [second order Process (3)], and several first-order quenching processes for  $O_2(^1\Delta)$  and  $I^*$ . In particular, we have considered the quenching of  $I^*$  by  $H_2O$ ,  $O_2(^3\Sigma)$ ,  $I$  atoms, and the walls. These processes have an increasingly important effect on draining the  $O_2(^1\Delta)$  storage reservoir as the  $I^*/O_2(^1\Delta)$  ratio increases.

The presence of  $I_2$  causes  $O_2(^1\Delta)$  removal by more complex processes. The  $O_2(^1\Delta)$  energy can be used by several mechanisms to break the  $I_2$  bond and to create free  $I$  atoms. The electronic equilibrium [Process (1)] occurs rapidly, so that the  $I^*$  density is determined by the  $[^1\Delta]/[^3\Sigma]$  ratio and the total  $I$  atom density. The mechanism for  $I_2$  dissociation by  $O_2^*$  is not completely defined, however, it is certainly represented by a class of processes that can be described as chain reactions with chain branching. These include Process (3a) followed by (18a), Process (21), and Process (22). All these mechanisms consume  $> 2 O_2(^1\Delta)$  molecules per  $I_2$  dissociated.

The use of  $O_2(^1\Delta)$  to create the  $I$  atom laser medium can be avoided if an external power source is used to create free  $I$  atoms. A brief description has been given of the excimer laser photolysis of  $HI$  to perform that function and to create the possibility of a repetitively pulsed version of the COIL system.

## REFERENCES

1. W. E. McDermott, N. R. Pchelkin, D. J. Benard, and R. R. Bousek, *Appl. Phys. Lett.* 32, 469 (1978).
2. D. J. Benard, W. E. McDermott, N. R. Pchelkin, and R. R. Bousek, *Appl. Phys. Lett.* 34, 40 (1979).
3. R. J. Richardson and C. E. Wiswall, *Appl. Phys. Lett.* 35, 138 (1979).
4. R. F. Heidner III, C. E. Gardner, G. I. Segal, and T. M. El-Sayed, *J. Phys. Chem.* 87, 2348 (1983).
5. J. B. Koffend, C. E. Gardner, and R. F. Heidner III, *J. Chem. Phys.* 80, 1861 (1984).
6. R. G. Derwent and B. A. Thrush, *Trans. Faraday Soc.* 67, 2036 (1971).
7. S. J. Arnold, M. Kubo, and E. A. Ogryzlo, *Adv. in Chem. Series* 77, 133 (1968).
8. G. A. Fisk and G. N. Hays, *J. Chem. Phys.* 77, 4965 (1982).
9. L. R. Martin, R. B. Cohen, and J. F. Schatz, *Chem. Phys. Lett.* 41, 394 (1976).
10. S. A. Lawton and A. V. Phelps, *J. Chem. Phys.* 69, 1055 (1978).
11. K. H. Becker, W. Groth, and U. Schurath, *Chem. Phys. Lett.* 8, 259 (1971).
12. R. G. O. Thomas and B. A. Thrush, *J. Chem. Soc. Faraday Trans. 2*, 71, 664 (1975).
13. R. G. Aviles, D. F. Muller, and P. L. Houston, *Appl. Phys. Lett.* 37, 358 (1980).
14. P. Borrell, P. M. Borrell, and M. D. Pedley, *Chem. Phys. Lett.* 51, 300 (1977).
15. A. Leiss, U. Schurath, K. H. Becker, and E. H. Fink, *J. Photochem.* 8, 211 (1978).
16. R. G. Derwent and B. A. Thrush, *Discuss. Faraday Soc.* 53, 162 (1972).
17. R. F. Heidner III, C. E. Gardner, T. M. El-Sayed, and G. I. Segal, *Chem. Phys. Lett.* 81, 142 (1981).
18. A. T. Young and P. L. Houston, *J. Chem. Phys.* 78, 2317 (1983).

19. R. F. Heidner III, C. E. Gardner, T. M. El-Sayed, G. I. Segal, and J. V. V. Kasper, *J. Chem. Phys.* 74, 5618 (1981).
20. D. H. Burde and R. A. McFarlane, *J. Chem. Phys.* 64, 1850 (1976).
21. A. J. Grimley and P. L. Houston, *J. Chem. Phys.* 69, 2339 (1978).
22. R. J. Donovan and D. Husain, *Trans. Faraday Soc.* 62, 2023 (1966).
23. G. Brederlow, E. Fill, and K. J. Witte, The High Power Iodine Laser, Springer Series in Optical Sciences, Vol. 34, Springer, Berlin, Heidelberg, New York (1983).
24. S. J. Arnold, N. Finlayson, and E. A. Ogryzlo, *J. Chem. Phys.* 44, 2529 (1966).
25. R. G. Derwent, D. R. Kearns, and B. A. Thrush, *Chem. Phys. Lett.* 6, 115 (1970).
26. R. G. Derwent and B. A. Thrush, *J. Chem. Soc. Faraday Trans. 2*, 68, 720 (1972).
27. D. F. Muller, R. H. Young, P. L. Houston, and J. R. Wiesenfeld, *Appl. Phys. Lett.* 38, 404 (1981).

## LABORATORY OPERATIONS

The Laboratory Operations of The Aerospace Corporation is conducting experimental and theoretical investigations necessary for the evaluation and application of scientific advances to new military space systems. Versatility and flexibility have been developed to a high degree by the laboratory personnel in dealing with the many problems encountered in the nation's rapidly developing space systems. Expertise in the latest scientific developments is vital to the accomplishment of tasks related to these problems. The laboratories that contribute to this research are:

Aerophysics Laboratory: Launch vehicle and reentry fluid mechanics, heat transfer and flight dynamics; chemical and electric propulsion, propellant chemistry, environmental hazards, trace detection; spacecraft structural mechanics, contamination, thermal and structural control; high temperature thermomechanics, gas kinetics and radiation; cw and pulsed laser development including chemical kinetics, spectroscopy, optical resonators, beam control, atmospheric propagation, laser effects and countermeasures.

Chemistry and Physics Laboratory: Atmospheric chemical reactions, atmospheric optics, light scattering, state-specific chemical reactions and radiation transport in rocket plumes, applied laser spectroscopy, laser chemistry, laser optoelectronics, solar cell physics, battery electrochemistry, space vacuum and radiation effects on materials, lubrication and surface phenomena, thermionic emission, photosensitive materials and detectors, atomic frequency standards, and environmental chemistry.

Computer Science Laboratory: Program verification, program translation, performance-sensitive system design, distributed architectures for spaceborne computers, fault-tolerant computer systems, artificial intelligence and microelectronics applications.

Electronics Research Laboratory: Microelectronics, GaAs low noise and power devices, semiconductor lasers, electromagnetic and optical propagation phenomena, quantum electronics, laser communications, lidar, and electro-optics; communication sciences, applied electronics, semiconductor crystal and device physics, radiometric imaging; millimeter wave, microwave technology, and RF systems research.

Materials Sciences Laboratory: Development of new materials: metal matrix composites, polymers, and new forms of carbon; nondestructive evaluation, component failure analysis and reliability; fracture mechanics and stress corrosion; analysis and evaluation of materials at cryogenic and elevated temperatures as well as in space and enemy-induced environments.

Space Sciences Laboratory: Magnetospheric, auroral and cosmic ray physics, wave-particle interactions, magnetospheric plasma waves; atmospheric and ionospheric physics, density and composition of the upper atmosphere, remote sensing using atmospheric radiation; solar physics, infrared astronomy, infrared signature analysis; effects of solar activity, magnetic storms and nuclear explosions on the earth's atmosphere, ionosphere and magnetosphere; effects of electromagnetic and particulate radiations on space systems; space instrumentation.

**END**

**FILMED**

---

*1-86*

**DTIC**